



Article

Characteristics and Source Identification for PM_{2.5} Using PMF Model: Comparison of Seoul Metropolitan Area with Baengnyeong Island

Kyoung-Chan Kim ¹ , Hui-Jun Song ¹, Chun-Sang Lee ¹ , Yong-Jae Lim ^{1,2}, Joon-Young Ahn ², Seok-Jun Seo ² and Jin-Seok Han ^{1,*}

¹ Department of Environmental Engineering, Anyang University, Anyang 14028, Republic of Korea; rudcksdldk@naver.com (K.-C.K.)

² Climate and Air Quality Research Department, National Institute of Environmental Research, Incheon 22689, Republic of Korea

* Correspondence: nierhan@hanmail.net; Tel.: +82-31-463-1292

Abstract: To establish and implement effective policies for controlling fine particle matters (PM_{2.5}), which is associated with high-risk diseases, continuous research on identifying PM_{2.5} sources was conducted. This study utilized the positive matrix factorization (PMF) receptor model to estimate the sources and characteristics of PM_{2.5} between Baengnyeong Island (BNI) and the Seoul Metropolitan Area (SMA). We conducted PMF modeling and backward trajectory analysis using the data on PM_{2.5} and its components collected from 2020 to 2021 at the Air quality Research Centers (ARC). The PMF modeling identified nine pollution sources in both BNI and the SMA, including secondary sulfate, secondary nitrate, vehicles, biomass burning, dust, industry, sea salt particles, coal combustion, and oil combustion. Secondary particulate matter, vehicles, and biomass burning were found to be major contributors to PM_{2.5} concentrations in both regions. A backward trajectory analysis indicated that air masses, passing through BNI to the SMA, showed higher concentrations and contributions of ammonium nitrate, vehicles, and biomass burning in the SMA site compared to BNI site. These findings suggest that controlling nitrogen oxides (NO_x) and ammonia emissions in the SMA, as well as monitoring the intermediate products that form aerosols, such as HNO₃, are needed.

Keywords: PM_{2.5}; source apportionment; PMF; Baengnyeong Island; Seoul Metropolitan Area; nitrate source



Citation: Kim, K.-C.; Song, H.-J.; Lee, C.-S.; Lim, Y.-J.; Ahn, J.-Y.; Seo, S.-J.; Han, J.-S. Characteristics and Source Identification for PM_{2.5} Using PMF Model: Comparison of Seoul Metropolitan Area with Baengnyeong Island. *Atmosphere* **2024**, *15*, 1146. <https://doi.org/10.3390/atmos15101146>

Academic Editor: Antonio Donateo

Received: 31 August 2024

Revised: 21 September 2024

Accepted: 23 September 2024

Published: 24 September 2024



Copyright: © 2024 by the authors. Licensee MDPI, Basel, Switzerland. This article is an open access article distributed under the terms and conditions of the Creative Commons Attribution (CC BY) license (<https://creativecommons.org/licenses/by/4.0/>).

1. Introduction

Fine particulate matter (PM_{2.5}) comes from natural sources like fugitive dust but is also heavily emitted by human activities, such as vehicle emissions, industry, and combustion. These sources significantly affect air quality and public health. PM_{2.5} is currently a key area of research to understand its sources and impacts for effective mitigation [1,2]. Recent studies analyzing the chemical composition of PM_{2.5} revealed that ionic components constitute the largest proportion, leading to an increased interest in the secondary pollutants formed through chemical reactions in the atmosphere [3–5].

The receptor model is one of the most widely used methods to study source apportionment of PM_{2.5} based on statistical analysis. The use of receptor models in atmospheric research was begun by Blifford and Meeker to calculate and address air pollution problems [6]. Receptor models allow for the estimation of pollution sources and the quantitative assessment of their contributions with observed data at the receptor site [7,8]. A multivariate receptor model, namely the positive matrix factorization (PMF) model, was developed by Paatero and Tapper to mitigate the limitations of factor analysis and has been continuously improved and updated over the years [9]. Anttila et al. conducted the first atmospheric study using the PMF model [10]. Polissar et al. and Ramadan et al. applied the

PMF model for source apportionment in Alaska and Phoenix, Arizona, respectively [11,12]. Han et al. estimated the sources of PM_{2.5} at a high-altitude region in South Korea (Korea) and applied a novel hybrid receptor model to assess contributions based on spatial information [13]. Recently, further advancements were made in receptor modeling by improving PMF-based hybrid models, which have enhanced the performance of the model [14,15].

The differences in characteristics and composition in PM_{2.5} are affected by various factors such as meteorological conditions, regional and seasonal characteristics, and so on [16]. The Seoul Metropolitan Area (SMA) has a very high population density and is an urban region with active traffic and commercial activities, which leads to complex patterns of PM_{2.5} distribution and emissions [17]. In particular, high concentrations of air pollutants are influenced by local primary emissions and the air currents of the prevailing westerlies into the SMA [18]. A recent case study showed that long-range transported pollutants, such as nitric acid (HNO₃), are formed and transported across the Yellow Sea, and entered the SMA [19]. The studies on these transboundary pollutants were consistently conducted to estimate the sources and identify characteristics of PM_{2.5} [20–23].

This study observed concentrations of PM_{2.5} and its components over a two-year period at the Air quality Research Center (ARC) in both a background site and an urban site. The characteristics and contributions of PM_{2.5} sources in these measurement sites were identified using the PMF receptor model. Additionally, a backward trajectory analysis was applied to classify the cases where long-range pollutants passed through BNI and transported into the SMA.

2. Experimental Methods of Analysis

2.1. Sampling and Observations

This study was conducted based on data observed at the ARC in two different regions, BNI and the SMA sites (Figure 1). The Baengnyeong ARC site (37.96° N, 124.63° E) is situated the northernmost region of Korea, approximately halfway between Korea and China. BNI is well suited for monitoring and analyzing the movement of long-range pollutants, with minimal interference from anthropogenic sources, playing a role as the site of ambient background concentrations. The Seoul ARC in Bulgwang-dong (37.61° N, 126.933° E) focuses on monitoring and analyzing complex air pollution of high-concentration pollution from traffic and commercial activities in this densely populated area. The measurements at both sites were conducted over a two-year period, from 1 January 2020, to 31 December 2021.

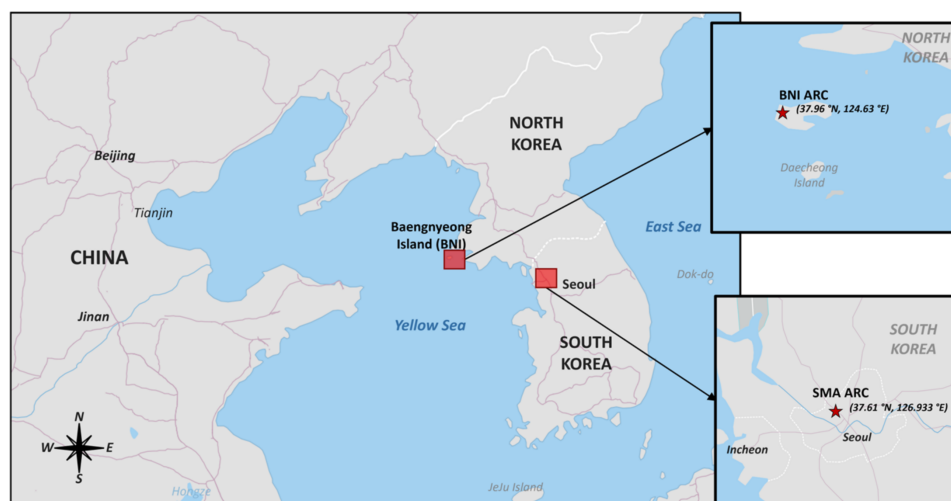


Figure 1. Sampling sites in Air quality Research Center (ARC) at Baengnyeong Island (BNI) and Seoul Metropolitan Area (SMA).

The measurement data were based on hourly averages over the study period. The observed species included the mass concentration ($\mu\text{g m}^{-3}$) of $\text{PM}_{2.5}$ and its components: 8 ionic species (such as SO_4^{2-} , NO_3^- , and NH_4^+), carbonaceous species (organic carbon (OC) and elemental carbon (EC)), and 15 heavy metals (such as Pb, Cr, Cu, and so on), and their method detection limits (MDLs) were shown in Table 1. $\text{PM}_{2.5}$ mass concentrations were measured using a beta attenuation monitor (BAM-1020, MetOne Instrument Inc., Grants Pass, OR, USA) based on beta-ray absorption technique. Air samples were collected at a flow rate of 16.7 L min^{-1} . PM_{10} was separated via inertial impaction, and $\text{PM}_{2.5}$ was isolated using a cyclone. The separated $\text{PM}_{2.5}$ was collected on a Teflon filter for 42 min/h using a semi-online system. Ionic components were collected using an ambient ion monitor (AIM, URG-900D, URG Corporation, Chapel Hill, NC, USA), which were sampled for 55 min/h. The collected samples were then analyzed using ion chromatography (IC, ICS-2000, DIONEX, Sunnyvale, CA, USA). For carbonaceous components, samples were collected at a flow rate of 8 L min^{-1} for 45 min and analyzed using an OC/EC analyzer (Model-4, Sunset Laboratory Inc., Tigard, OR, USA) that employed thermal-optical and non-dispersive infrared (NDIR) methods. Metal species were measured using an XRF spectrometer (Xact 625i, SailBri Cooper Inc., Tigard, OR, USA), which utilized a non-destructive method to measure the wavelength and intensity of characteristic fluorescent X-rays. The detailed measurement methods and conditions for each instrument refer to the guidelines for the installation and operation of air pollution monitoring networks provided by the National Institute of Environmental Research (NIER) of Korea [24].

Table 1. Method detection limits ($\mu\text{g m}^{-3}$) for components of $\text{PM}_{2.5}$.

Components	MDLs	Components	MDLs
$\text{PM}_{2.5}$	5	K	0.00117
SO_4^{2-}	0.1	Ca	0.00030
NO_3^-	0.1	Ti	0.00016
NH_4^+	0.1	Cr	0.00012
OC	0.5	Mn	0.00014
EC	0.5	Fe	0.00017
		Cu	0.00008
		Zn	0.00007
		As	0.00006
		Br	0.00010
		Pb	0.00013

2.2. PMF Receptor Models

Receptor models use techniques such as factor analysis, regression models, and so on to identify pollution sources and access their contributions at the receptor site, even without prior information on the sources or emissions. The PMF receptor model is particularly notable for its ability to handle mixed and overlapping sources. It ensures that source contributions remain positive and optimizes the solution by minimizing the sum of squared residuals [9]. PMF also accounts for data uncertainty, offering improved accuracy over traditional factor analysis models. The basic equation is shown in Equation (1).

$$X = G \times F + E \quad (1)$$

The matrix X represents a data matrix composed of n samples and m variables. G is an $n \times p$ matrix that denotes the contribution of sources, where p represents the number of sources. F is a $p \times m$ matrix indicating the source profile, and E is the residual matrix. Both G and F are calculated as positive values using the least squares method, with E minimized as a result. In this study, we used the latest version of the EPA PMF 5.0 model developed by the US EPA. The PMF model may be influenced by user decisions during data preprocessing or source estimation, which can introduce subjectivity and affect the reliability of the results. To mitigate this and standardize model operation, the National Institute of Environmental

Research (NIER) has established guidelines for data preprocessing and the use of the PMF program. Following these guidelines, this study conducted pretreatments of data (i.e., outlier processing, ion balance assessment, and calculation uncertainty) [25]. Missing values were replaced with the median of the data, and the uncertainty for each measurement was calculated based on the method detection limits (MDLs) and the equation provided (Equation (2)).

$$Uncertainty = \begin{cases} MDL \times \frac{5}{6}, & C_i < MDLs \\ Median \times 4, & \text{Missing value} \\ \sqrt{(C_i \times \text{error fraction})^2 + (MDL \times 0.5)^2}, & C_i \geq MDLs \end{cases} \quad (2)$$

where C_i represents the concentration ($\mu\text{g m}^{-3}$) of each species, and an error fraction was applied at 10% in this study. The MDLs for each species are provided in Table 1.

2.3. Back-Trajectory Analysis

Korea is located downwind in the westerly wind belt, where it is susceptible to long-range transported pollutants. Therefore, tracking those movements of air masses by backward trajectory analysis is crucial. In this study, the backward trajectory model was used to analyze long-range transported pollutants [26–28]. The hybrid single particle Lagrangian integrated trajectory (HYSPLIT) model was employed to trace the pathways of air pollutants and wind from external sources [29], using meteorological data from the global data assimilation system (GDAS1) archive to analyze the backward trajectories. The simulation period for the trajectories was set to 72 h (3 days), with a reference altitude of 500 m.

The analysis focused on air masses entering BNI and the SMA from the northwest. We selected cases where the trajectories passed over BNI and then reached the SMA. Trajectories crossing above 37.61° N and below 126.93° E were initially identified. Among these, those passing through BNI before arriving in the SMA were further categorized. Measurements from the two sites corresponding to these selected cases were aligned and compared.

3. Results and Discussion

3.1. Concentrations of $PM_{2.5}$ and Its Components

Table 2 presents the statistical summary of $PM_{2.5}$ mass concentrations and components measured over two years at BNI and the SMA. The average $PM_{2.5}$ mass concentrations in the SMA ($21.7 \pm 16.4 \mu\text{g m}^{-3}$) were higher than those in BNI ($19.8 \pm 16.8 \mu\text{g m}^{-3}$) due to various anthropogenic activities in the SMA. During the analysis period, yellow dust events occurred 19 and 20 times in BNI and the SMA, respectively. Aside from these events, high $PM_{2.5}$ concentrations were defined as periods where the concentration exceeded $36 \mu\text{g m}^{-3}$ for more than 1 h, as shown in Figure 2. Most high concentration events occurred during winter, likely driven by air masses passing over BNI and into the SMA.

$PM_{2.5}$ observed at BNI was composed of approximately 61% ionic species, 12% carbons, and 11% metals. In contrast, the $PM_{2.5}$ composition at the SMA consisted of 50% ions, 18% carbons, and 10% metals. In both sites, ionic species such as nitrate, sulfate, and ammonium ions made up the largest fraction, and the fractions of ions in BNI were higher compared to those in the SMA (Figure 3). Among the ionic species, sulfate and ammonium had higher proportions at BNI, while nitrate levels were nearly equivalent in both sites. This suggested that secondary aerosol formation played a significant role in $PM_{2.5}$ pollution at BNI, a background site. In the SMA, heavy metals and OC were at higher levels, indicating a substantial influence from primary emissions, likely due to industrial activities or fuel combustion.

Table 2. Summary of PM_{2.5} and its components measured in BNI and the SMA (units: µg m^{−3}).

		PM _{2.5}	SO ₄ ^{2−}	NO ₃ [−]	Cl [−]	Na ⁺	NH ₄ ⁺	K ⁺	Mg ²⁺	Ca ²⁺	Cation	Anion	Ion	Ion/PM _{2.5}	OC	EC	Carbon	Carbon/PM _{2.5}	Metal	Metal/PM _{2.5}
BNI	<i>n</i>	16,447	12,559	12,505	11,866	12,565	12,565	12,565	12,564	12,552	17,545	17,545	17,545	16,439	14,576	14,571	17,545	16,439	17,544	16,439
	AVG	19.8	3.9	4.8	0.3	0.1	2.9	0.1	0.0	0.0	3.2	9.0	12.2	0.61	1.9	0.4	2.3	0.12	2.1	0.11
	Max	273	38.5	74.7	3.3	2.5	30.7	5.3	0.5	1.5	31.5	115	147	4.6	16.0	3.4	19.4	1.6	26.0	1.5
	Min	1.0	0.0	0.0	0.0	0.0	0.0	0.0	0.0	0.0	0.0	0.0	0.1	0.0	0.0	0.0	0.0	0.0	0.0	0.0
	Median	15.0	2.9	1.4	0.2	0.1	1.6	0.1	0.0	0.0	1.2	3.1	4.3	0.4	1.5	0.3	1.4	0.1	1.6	0.1
	SD	16.8	3.6	8.3	0.4	0.2	3.5	0.2	0.0	0.1	3.4	10.4	13.7	0.3	1.6	0.4	2.0	0.1	2.1	0.1
SMA	<i>n</i>	16,847	15,452	15,458	15,456	15,458	15,460	15,037	15,454	15,387	17,545	17,545	17,545	16,835	15,631	15,631	17,545	16,835	17,545	16,835
	AVG	21.7	2.9	4.9	0.2	0.1	2.6	0.1	0.0	0.1	2.8	8.1	10.9	0.50	3.0	0.7	3.4	0.18	1.9	0.10
	Max	152	22.0	52.5	8.0	1.1	18.6	0.6	0.2	2.5	19.4	65.0	84.3	4.8	16.9	11.0	19.9	2.1	12.0	1.8
	Min	1.0	0.0	0.0	0.0	0.0	0.0	0.0	0.0	0.0	0.0	0.0	0.0	0.0	0.0	0.0	0.0	0.0	0.0	0.0
	Median	18.0	2.1	2.2	0.1	0.0	1.6	0.0	0.0	0.0	1.5	4.3	5.8	0.4	2.7	0.6	3.0	0.2	1.6	0.1
	SD	16.4	2.5	6.5	0.3	0.1	2.7	0.1	0.0	0.1	2.8	8.1	10.9	0.2	1.9	0.5	2.5	0.1	1.5	0.1

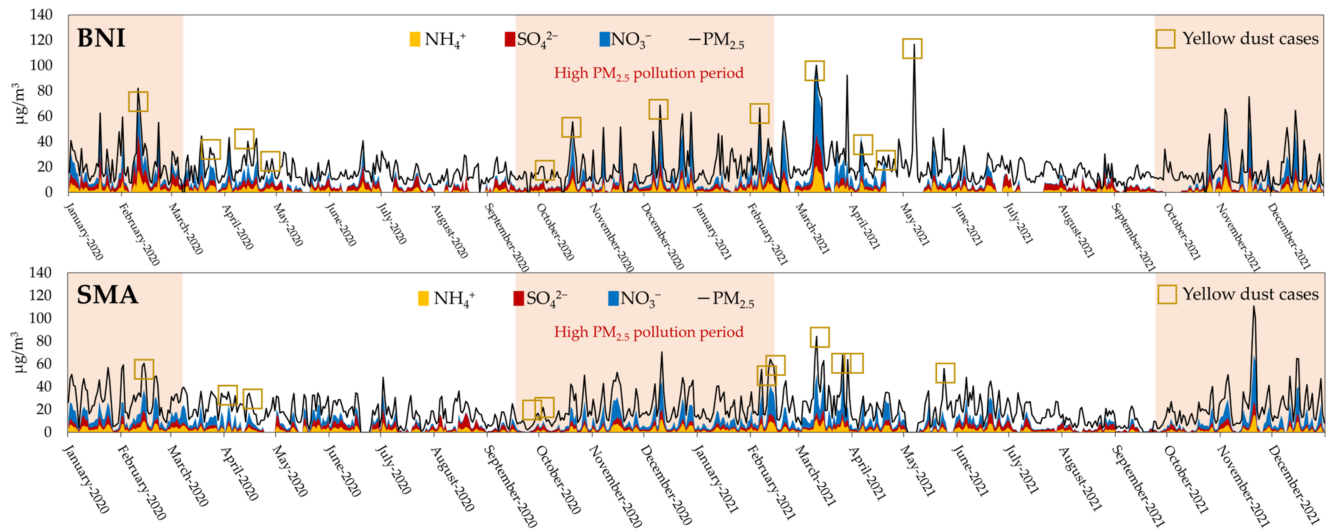


Figure 2. Time series distributions of $PM_{2.5}$ (black line), ammonium ions (yellow area), sulfate ions (red area), and nitrate ions (blue area) in BNI and the SMA. The brown boxes and the pink backgrounds represent the yellow dust cases and high $PM_{2.5}$ pollution periods, respectively.

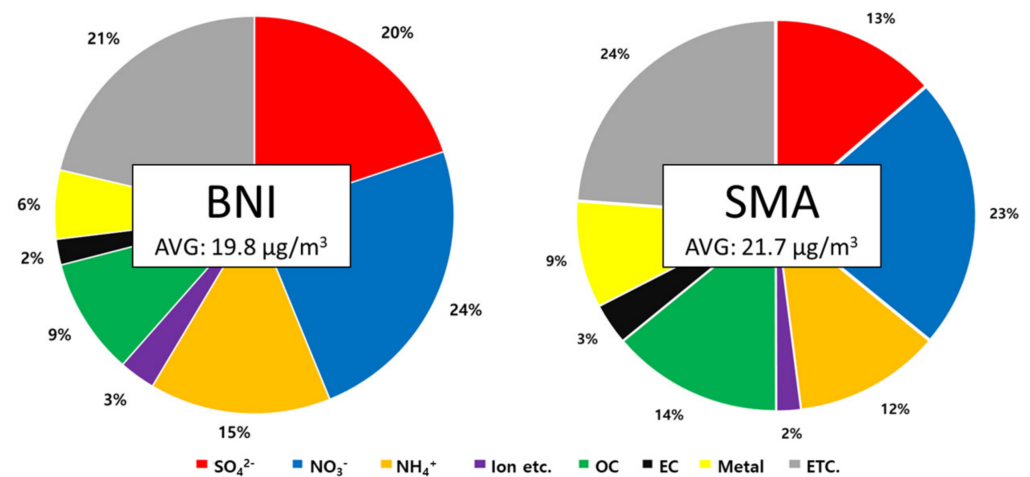


Figure 3. Composition for major components $PM_{2.5}$.

Figure 4 shows the average composition ratios of $PM_{2.5}$ components at each site, grouped by $PM_{2.5}$ concentration levels. As $PM_{2.5}$ concentration increased at both BNI and the SMA, the fraction of nitrate significantly increased. In the concentration range of 15 to $30 \mu g m^{-3}$, which aligned the average mass concentrations (BNI: $19.8 \mu g m^{-3}$, SMA: $21.7 \mu g m^{-3}$), the nitrate ion proportion increased by 23 percentage points at BNI and 15 percentage points at the SMA as concentrations approached $60 \mu g m^{-3}$. Additionally, ammonium ions also showed a proportional increase with higher $PM_{2.5}$ levels. A linear relationship was observed, with both the mass concentration and proportion of nitrate and ammonium ions increasing as $PM_{2.5}$ levels rose. As shown in Figure 2, high concentration events predominantly occurred in the winter, indicating aerosol formation of the secondary pollutant, such as NH_4NO_3 .

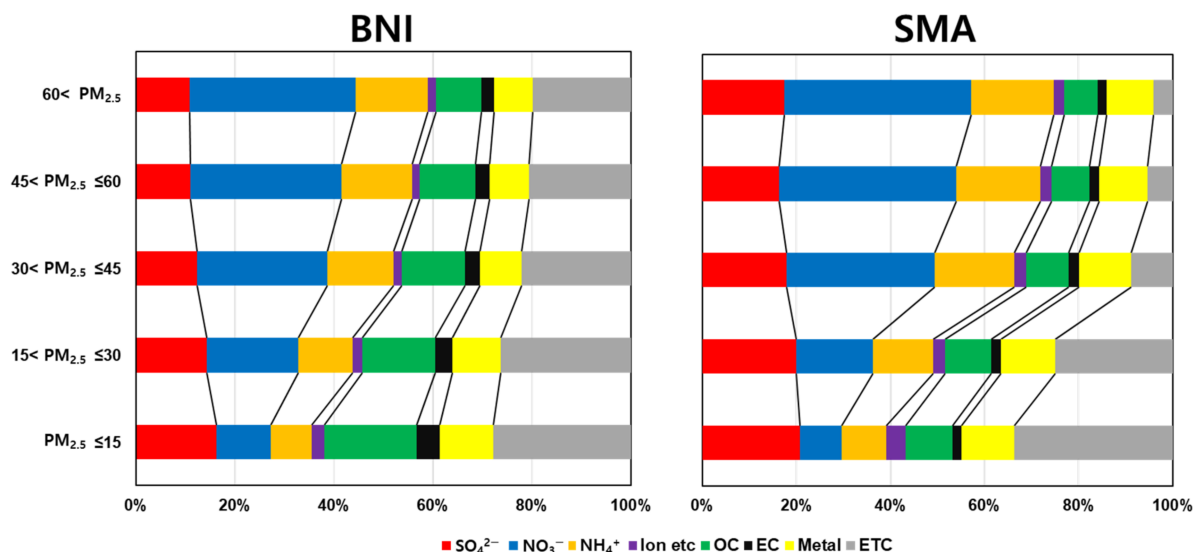


Figure 4. Fraction for components of $PM_{2.5}$ by mass concentration levels.

3.2. Pretreatment for Receptor Model

Figure 5 presents the correlation analysis plots of $PM_{2.5}$ and the mass equivalent concentrations of major ionic species (nitrate, sulfate, chloride, and ammonium ions), used for preprocessing PMF input data and ion balance. The ion balance between anions and cations shows a strong correlation with a slope close to 1:1, and the time series of major ionic components exhibited a strong correlation with those of $PM_{2.5}$ mass concentrations, indicating the significant role of secondary aerosol formation.

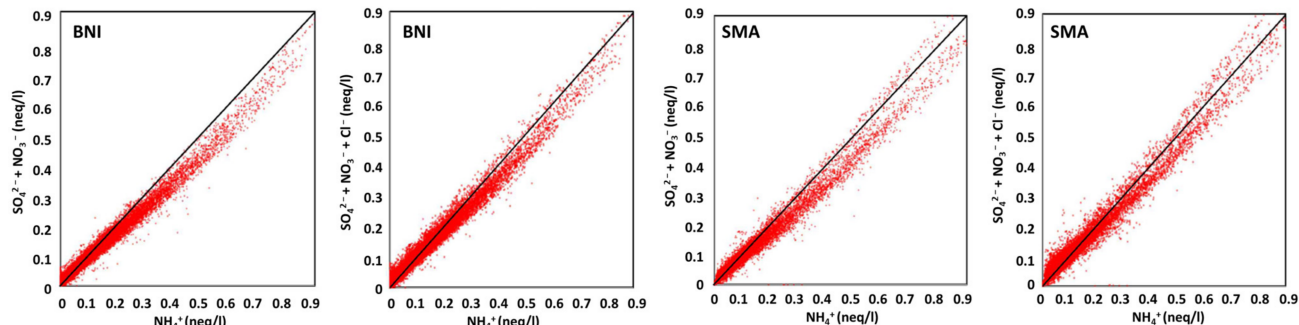


Figure 5. Correlation for major chemical ions in $PM_{2.5}$ at BNI and the SMA.

For data measured at BNI site, 9986 data points (57% of the raw data) were used, and their averaged $PM_{2.5}$ concentrations was $20.7 \pm 15.1 \mu\text{g m}^{-3}$. In the SMA, 12,668 data points (72% of the raw data) were utilized, resulting in an averaged $PM_{2.5}$ mass concentration of $24.0 \pm 16.9 \mu\text{g m}^{-3}$. The categorization process in the PMF model, which affects the accuracy of the model, was primarily determined based on the signal-to-noise (S/N) ratio. Following the initial model run, the categorization was finalized by considering several factors, including the correlation coefficient between observed and modeled values, the presence of source-specific tracers, and the number of data points below the MDLs or missing value. Consequently, the weak category included six species (such as Na^+ , EC, Ti, Cu, Zn, and Br) in BNI and four species (such as Na^+ , Cu, Zn, and Pb) in the SMA, respectively. Considering the redundancy among variables, the reliability of the data, and the model result of the base run, a few species (K^+ , Mg^{2+} , Ca^{2+} , S, V, and Cr in BNI and K^+ , Mg^{2+} , Ca^{2+} , S, V, Se, and Br in the SMA) were categorized in the bad group, and others were classified as the strong group. Figure 5 shows the correlation between the predicted and observed variables $PM_{2.5}$ and key component concentrations. The coefficients of determination (R^2) for the correlation between modeled and observed

PM_{2.5} (total variables) concentrations were 0.94 for BNI and 0.955 for the SMA, which indicated that the model could explain over 94% of the observed variations (Figure 6). Furthermore, excluding the chemical species categorized as weak, most components also had R² values above 0.7, indicating that the model reliably explains the variations in observed concentrations.

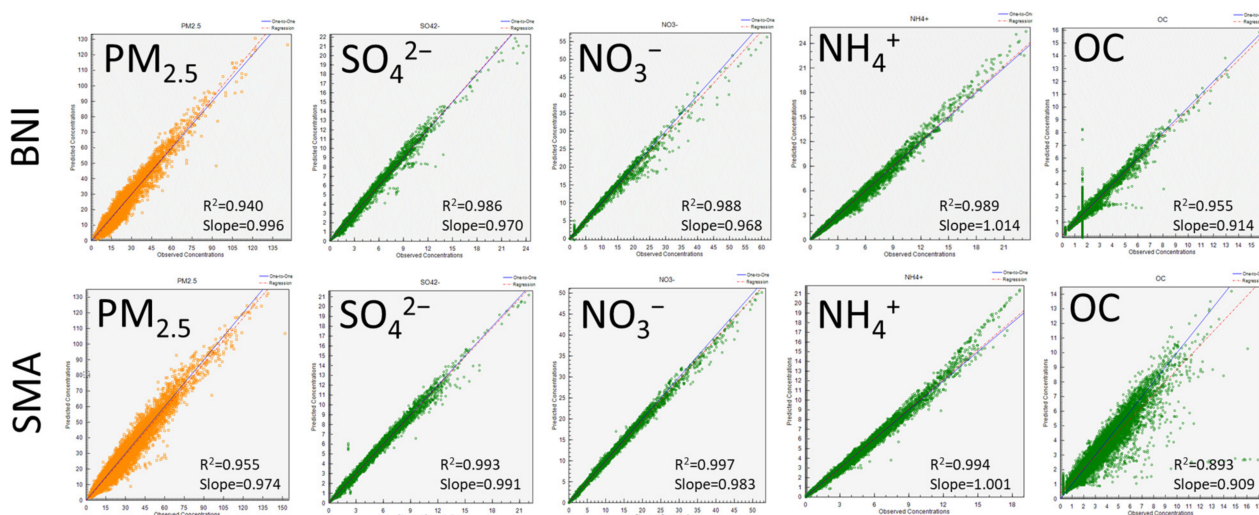


Figure 6. Correlation for each variation of PMF. Yellow and green dots represent weak and strong categories, respectively.

3.3. Source Apportionment of PMF Analysis

The sources contributing to ambient PM_{2.5} concentrations at BNI and the SMA were identified based on the species profiles utilizing the PMF model. In both sites, nine sources were identified, including secondary sulfate, secondary nitrate, vehicle emissions, industrial emissions, biomass burning, sea salt particles, soil and dust, coal combustion, and oil combustion. The profiles and contributions of the identified sources in each site are presented in Figure 7 and Table 3.

With NH₄⁺ and SO₄²⁻ as key indicators, secondary sulfate contributed 30% and 23% of the entire PM_{2.5} in BNI and the SMA, respectively, showing the largest proportion in BNI. Secondary sulfate is generally known to be primarily emitted during the winter due to the oxidation of SO₂, which is associated with the extensive use of sulfur-containing fossil fuels such as coal [30]. Secondary nitrate characterized by NH₄⁺ and NO₃⁻, accounted for 26% of the total PM_{2.5} in BNI and 27% in the SMA, respectively, which indicated significant contributions in both regions. Vehicle emissions were marked by OC, EC, Cu, and Zn and contributed 16% and 13% in BNI and the SMA, respectively. OC and EC are primarily emitted from gasoline and diesel exhaust, and a previous study suggested that Cu and Zn are dispersed mainly from brake abrasion on vehicle pedals [31]. Biomass burning was the third-largest contributing source in the SMA, accounting for 22% of the total PM_{2.5}. In contrast, its contribution was lower at BNI, where it accounted for 8%. Biomass burning is identified by the significant contributions of OC, EC, K, and Pb and typically results from activities like crop residue burning after harvest and wood combustion. This source generally shows a higher contribution during the winter season [32]. Fe, Ni, Zn, Se, and Br are known as key indicators of industrial emissions, contributing 5% and 7% of the total at BNI and the SMA, respectively [33]. Sea salt particles, originated from natural sources such as breaking waves, are characterized by high contributions of Na⁺ and Cl⁻ and contributed equally at 4% to the total PM_{2.5} in both BNI and the SMA [34]. Ti, Mn, Fe, and Ca are key indicators of dust emissions, heavily influenced by yellow dust carried by westerly winds. These components typically show higher contributions during the spring and autumn seasons, particularly during yellow dust events [15]. The contribution of soil and dust emissions, indicated by Ti, Mn, Fe, and Ca was relatively low, accounting for 5% at BNI

and 4% at the SMA. Coal combustion, characterized by As and Pb, contributed 3% at BNI, with higher contributions during winter and early spring, likely due to an increased use for heating purposes [35]. The last source was identified as oil combustion, which showed a relatively low contribution of 3% at BNI. Previous studies used Ni and V as key indicators of oil combustion emissions; however, in this study, V was excluded due to its classification as a bad variable, and only Ni was used to improve model reliability [36]. The contribution of coal and oil combustion sources in the SMA was negligible, both below 0.1%.

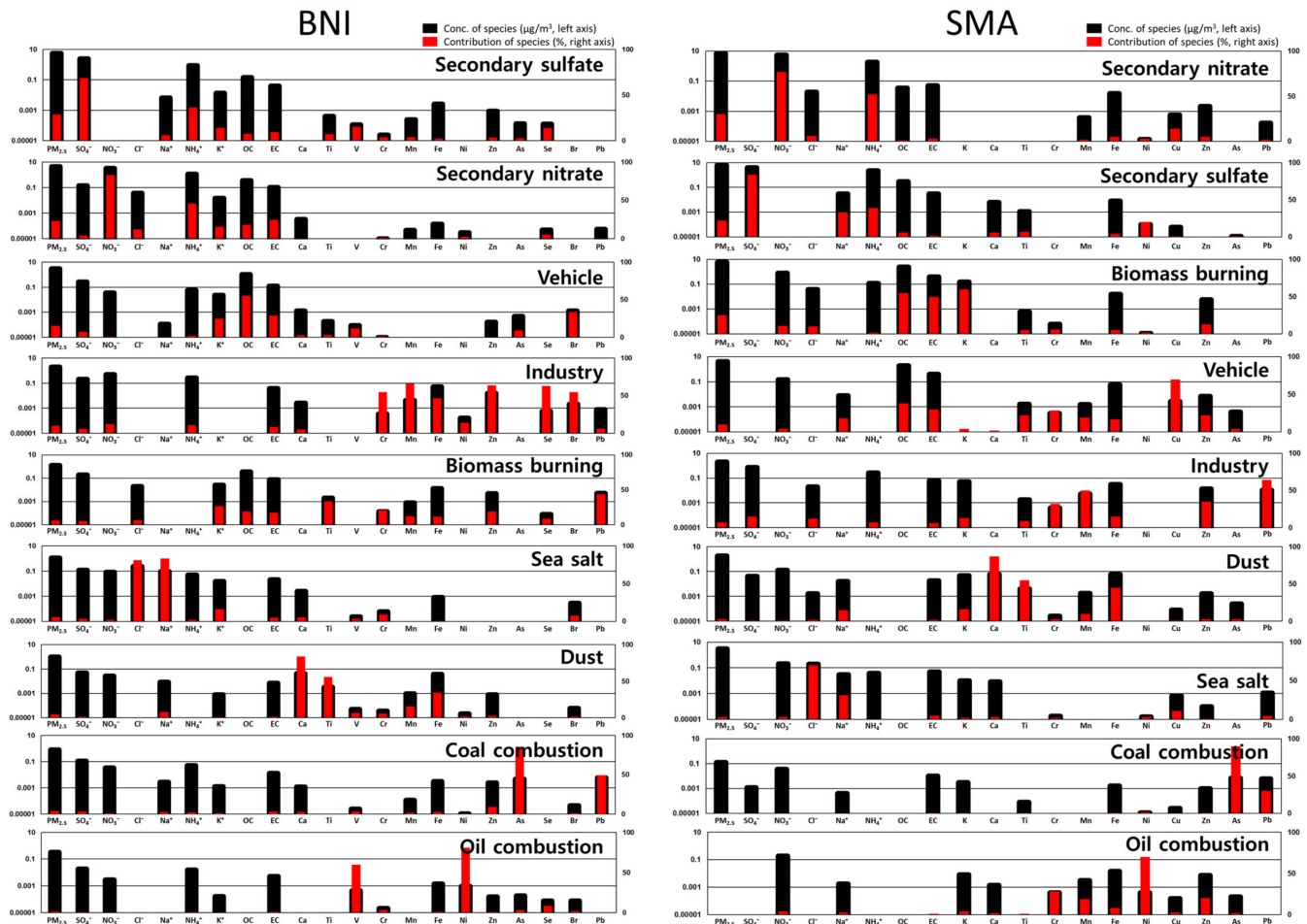


Figure 7. Source apportionments by using PMF model at BNI and the SMA.

Table 3. Contribution of PM_{2.5} sources.

Source	Contribution	
	BNI	SMA
Secondary sulfate	30%	23%
Secondary nitrate	26%	27%
Vehicle	16%	13%
Biomass burning	8%	22%
Industry	5%	7%
Dust	5%	4%
Sea salt	4%	4%
Coal combustion	3%	0.1%
Oil combustion	3%	0.1%

3.4. Backward Trajectory and Cluster Analysis

A backward trajectory analysis was conducted based on the data from the SMA, and the results of the trajectory cluster analysis are presented in Figure 8. The analysis indicated that 25% of the air masses entering the SMA originated from northeastern continental regions while 36.3% came from neighboring regions to the northwest. This suggests a significant influence of long-range transported pollutants from these regions on the air quality in the SMA.

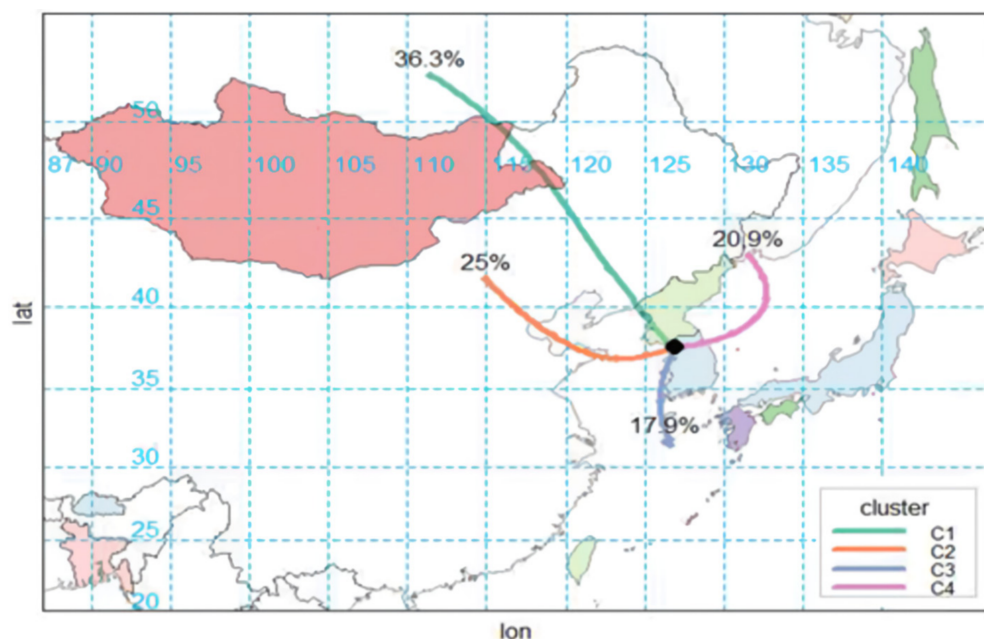


Figure 8. Clustering analysis for back trajectories.

In this study, trajectories passing through BNI before reaching the SMA were classified as case studies, with a total of 48 case days identified. The $\text{PM}_{2.5}$ concentrations at both BNI and the SMA for these classified air mass trajectories were compared and are presented in Table 4. The average $\text{PM}_{2.5}$ concentration of the cases was $10.3 \mu\text{g m}^{-3}$ higher when the pollutants reached the SMA compared to those measured at BNI. This suggests that as the air mass moved between BNI and the SMA, particularly during its passage through these two locations, there was a noticeable increase in pollutant concentration. Along with $\text{PM}_{2.5}$, the average mass concentrations of most components also increased. Notably, the concentrations of NO_3^- , NH_4^+ , and OC were $4.9 \mu\text{g m}^{-3}$, $1.45 \mu\text{g m}^{-3}$, and $1.78 \mu\text{g m}^{-3}$ higher in the SMA compared to BNI, corresponding to percentage increases of 134.1%, 70.4%, 115.6%, respectively.

In the PMF model results for the classified cases, the contributions from secondary nitrate, secondary sulfate, biomass burning, vehicle emissions, industrial emissions, and sea salt were higher (Table 5). Specifically, in the SMA, the contributions of secondary nitrate and biomass burning were $5.7 \mu\text{g m}^{-3}$ and $4.0 \mu\text{g m}^{-3}$ higher, respectively, compared to BNI, representing percentage increases of 135.71% and 235.29%, respectively. The contribution from vehicle emissions also showed a slight increase of $0.7 \mu\text{g m}^{-3}$. On the other hand, the contributions from dust, coal combustion, and oil combustion sources were lower in the SMA.

Table 4. Comparison of measured values (units: $\mu\text{g m}^{-3}$) in cases.

Species	BNI (a)	SMA (b)	Variation (b – a)
PM _{2.5}	16.2	26.5	+10.3
SO ₄ ^{2−}	2.91	3.21	+0.30
NO ₃ [−]	3.05	7.14	+4.09
Cl [−]	0.28	0.30	+0.02
Na ⁺	0.11	0.06	−0.05
NH ₄ ⁺	2.06	3.51	+1.45
K ⁺	0.07	0.07	
Mg ²⁺	0.02	0.02	
Ca ²⁺	0.03	0.06	+0.03
OC	1.54	3.32	+1.78
EC	0.32	0.78	+0.46
S	1.76	1.69	−0.07
K	0.16	0.21	+0.05
Ca	0.04	0.06	+0.02
Ti	0.00	0.01	+0.01
V	0.00	0.00	
Cr	0.00	0.00	
Mn	0.01	0.01	
Fe	0.10	0.17	+0.07
Ni	0.00	0.00	
Cu	0.00	0.01	+0.01
Zn	0.02	0.04	+0.02
As	0.01	0.01	
Se	0.00	0.00	
Br	0.00	0.01	+0.01
Pb	0.01	0.01	

Table 5. Comparison of contribution values (units: $\mu\text{g m}^{-3}$) for sources by PMF in cases.

Sources	BNI (a)	SMA (b)	Variation (b – a)
Total (PM _{2.5})	17.5	29.0	+11.5
Secondary sulfate	5.0	5.8	+0.8
Secondary nitrate	4.2	9.9	+5.7
Vehicle	2.6	3.3	+0.7
Biomass burning	1.7	5.7	+4.0
Dust	0.9	0.9	
Industry	1.0	2.1	+1.1
Sea salt	0.7	1.2	+0.4
Coal combustion	0.8	0.2	−0.6
Oil combustion	0.5	<0.1	−0.4

3.5. Discussion

In cases where long-range transported pollutants entered the SMA after passing through BNI and the Yellow Sea, higher concentrations of air pollutants were observed in the SMA compared to BNI. This observation suggests the presence of additional pollution sources along the air mass trajectory between these regions. Given that BNI serves as a background site with minimal local emissions, it is evident that supplementary sources within the SMA contributed to the increased PM_{2.5} levels [37].

In Korea, air pollutant emissions data are reported annually by the Clean Air Policy Support System (CAPSS). This study focused on the emissions data from Seoul, Gyeonggi, and Incheon, which correspond to the SMA (Table 6). For comparison with the categorized source factors in this study, road and non-road mobile sources were combined as the vehicle source, while energy industry combustion, production processes, energy transport and storage, and waste management were combined as the industry source. The biomass burning source was categorized directly as biomass burning. Through the CAPSS data, it

was confirmed that the air pollutants identified in this study were indeed emitted from the classified sources, and additional sources were identified. Particularly, emissions from sources with high contributions to the SMA, such as secondary sulfate, secondary nitrate, vehicle emissions, and biomass burning, were found to significantly impact PM_{2.5} pollution.

Table 6. The emissions (units: ton/yr) of pollutants from vehicle, industry, and biomass burning sources.

Emission Source		Vehicle	Industry	Biomass Burning
2020 year	NO _x	195,773	23,287	874
	SO _x	1325	10,667	12
	PM _{2.5}	5170	1091	1817
	NH ₃	866	6231	2
	BC	3,35,	243	276
2021 year	NO _x	181,372	23,728	831
	SO _x	584	9326	12
	PM _{2.5}	4579	1217	1840
	NH ₃	702	6653	2
	BC	2902	278	276

The results of the measurements and source apportionments and the formation of ammonium nitrate (NH₄NO₃) significantly influences PM_{2.5} pollution in the SMA. There are previous studies on various factors contributing to the formation of ammonium nitrate aerosols.

Kang et al. (2018) reported that the combustion of fossil fuels, leading to SO_x pollution, can reduce atmospheric acidity and promote the evaporation of nitrate, thereby increasing gaseous HNO₃ concentrations during the winter season [38]. In such cases, HNO₃ likely remains in its gaseous form over the Yellow Sea, where NH₃ emissions are minimal. As the air mass reaches NH₃ local sources on the SMA, a heterogenous reaction between gaseous HNO₃ and HN₃ actively occurs, which leads to the formation of NH₄NO₃ [39]. Park et al. (2024) enhanced the accuracy of their model for simulating PM_{2.5} concentrations in the SMA by incorporating the formation of NH₄NO₃, thereby confirming the long-range transport potential of HNO₃ gas and its significant impact on PM_{2.5} pollution in the SMA [19]. Zhang et al. (2024) reported that the wintertime increases in NO₃ gas in China, influenced by photochemical reactions involving ozone (O₃), plays a crucial role in nitrate formation [40]. Similarly, Lee (2019) found that as air masses from eastern and northeastern regions expanded, PM_{2.5} concentrations and nitrogen-oxygen isotope ratios in the SMA increased [27].

Furthermore, it is assumed that the NO_x sources in the SMA affect the higher concentrations of OC and EC in the SMA compared to BNI, along with the higher contribution from vehicle emissions. The vehicle sources likely contribute significantly to NO_x pollution, which converts to HNO₃ in the atmosphere and reacts with NH₃ to form aerosols [41,42]. These findings highlighted the importance of managing ammonia and NO_x emissions within the SMA to control PM_{2.5} pollution.

While this study focused on comparing the background region of BNI and the densely populated SMA, additional case studies are needed for central and southwestern regions of Korea, which are adjacent to the Yellow Sea and have high ammonia emissions. Future research should also analyze the impact of biomass burning on PM_{2.5} concentrations, particularly considering biomass burning as a significant source of ammonia emissions.

4. Conclusions

This study examined the characteristics of PM_{2.5} and its components in BNI and the SMA from 2020 to 2021 and estimated the emission sources. Additionally, utilizing a trajectory analysis, we identified changes in the characteristics of long-range transported pollutants as they moved from BNI to the SMA, leading to the following implications.

1. During the measurement period, the average PM_{2.5} mass concentrations were $19.8 \pm 16.8 \mu\text{g m}^{-3}$ at BNI and $21.9 \pm 16.4 \mu\text{g m}^{-3}$ in the SMA. This indicates that a wider variety of emission sources contributed to fine particle pollution in the urban region (SMA) compared to the background region (BNI).
2. In both sites, sulfate and nitrate were the dominant components of PM_{2.5}, and as the PM_{2.5} concentration increased, the relative proportion of nitrate also rose. It suggests that heterogeneous reactions between gaseous nitric acid and ammonia in the atmosphere were likely enhanced, leading to the formation of ammonium nitrate aerosols.
3. The PMF model analysis of PM_{2.5} sources identified nine sources at BNI, and secondary sulfate (30%) and secondary nitrate (26%) were dominant sources. Similarly, nine sources were identified in the SMA, and secondary nitrate (27%), secondary sulfate (23%), and biomass burning (22%) were dominant contributors.
4. A comparative analysis of BNI and the SMA in cases where air masses moved from BNI to the SMA revealed that the contributions of secondary pollutants (sulfate and nitrate), biomass burning, and vehicle emissions were higher in the SMA than in BNI. The increase in secondary pollutants is likely due to the HNO₃ being transported via BNI and converted from NO_x by local vehicles, which then reacted with additional NH₃ from domestic sources.

These findings highlight the importance of managing local sources of NH₃ and NO_x in the SMA and surrounding regions. Additionally, for effective and scientific control of PM_{2.5} pollution in Korea, further research is needed to better understand the characteristics of long-range transported pollutants entering the country via the BNI.

Author Contributions: Conceptualization, J.-S.H.; methodology, K.-C.K.; validation, J.-S.H., S.-J.S. and J.-Y.A.; formal analysis, K.-C.K., H.-J.S. and C.-S.L.; investigation, K.-C.K. and H.-J.S.; data curation, S.-J.S. and J.-Y.A.; writing—original draft preparation, K.-C.K. and Y.-J.L.; writing—review and editing, K.-C.K. and C.-S.L.; supervision, J.-S.H.; funding acquisition, J.-S.H. All authors have read and agreed to the published version of the manuscript.

Funding: This research and APC were funded by Experts Training Graduate Program for Particulate Matter Management from the Ministry of Environment, Korea.

Institutional Review Board Statement: Not applicable.

Informed Consent Statement: Not applicable.

Data Availability Statement: The data presented in this study are available on request from the corresponding author. The data are not publicly available due to privacy.

Conflicts of Interest: The authors declare no conflicts of interest.

References

1. Landrigan, P.J. Air Pollution and Health. *Lancet Public Health* **2017**, *2*, e4–e5. [[CrossRef](#)] [[PubMed](#)]
2. Dockery, D.W.; Stone, P.H. Cardiovascular Risks from Fine Particulate Air Pollution. *N. Engl. J. Med.* **2007**, *356*, 511–513. [[CrossRef](#)] [[PubMed](#)]
3. Choi, J.-K.; Heo, J.-B.; Ban, S.-J.; Yi, S.-M.; Zoh, K.-D. Chemical Characteristics of PM_{2.5} Aerosol in Incheon, Korea. *Atmos. Environ.* **2012**, *60*, 583–592. [[CrossRef](#)]
4. Glavas, S.D.; Nikolakis, P.; Ambatzoglou, D.; Mihalopoulos, N. Factors Affecting the Seasonal Variation of Mass and Ionic Composition of PM_{2.5} at a Central Mediterranean Coastal Site. *Atmos. Environ.* **2008**, *42*, 5365–5373. [[CrossRef](#)]
5. Yao, X.; Chan, C.K.; Fang, M.; Cadle, S.; Chan, T.; Mulawa, P.; He, K.; Ye, B. The Water-Soluble Ionic Composition of PM_{2.5} in Shanghai and Beijing, China. *Atmos. Environ.* **2002**, *36*, 4223–4234. [[CrossRef](#)]
6. Blifford, I.H.; Meeker, G.O. A Factor Analysis Model of Large Scale Pollution. *Atmos. Environ.* **1967**, *1*, 147–157. [[CrossRef](#)]
7. Hwang, I.; Kim, D.-S. Research Trends of Receptor Models in Korea and Foreign Countries and Improvement Directions for Air Quality Management. *J. Korean Soc. Atmos. Environ.* **2013**, *29*, 459–476. [[CrossRef](#)]
8. McMurry, P.H.; Shepherd, M.F.; Vickery, J.S. *Particulate Matter Science for Policy Makers: A NARSTO Assessment*; Cambridge University Press: Cambridge, UK, 2004; ISBN 978-0-521-84287-7.
9. Paatero, P.; Tapper, U. Positive Matrix Factorization: A Non-Negative Factor Model with Optimal Utilization of Error Estimates of Data Values. *Environmetrics* **1994**, *5*, 111–126. [[CrossRef](#)]

10. Anttila, P.; Paatero, P.; Tapper, U.; Järvinen, O. Source Identification of Bulk Wet Deposition in Finland by Positive Matrix Factorization. *Atmos. Environ.* **1995**, *29*, 1705–1718. [\[CrossRef\]](#)
11. Polissar, A.V.; Hopke, P.K.; Paatero, P.; Malm, W.C.; Sisler, J.F. Atmospheric Aerosol over Alaska: 2. Elemental Composition and Sources. *J. Geophys. Res. Atmos.* **1998**, *103*, 19045–19057. [\[CrossRef\]](#)
12. Ramadan, Z.; Song, X.-H.; Hopke, P.K. Identification of Sources of Phoenix Aerosol by Positive Matrix Factorization. *J. Air Waste Manag. Assoc.* **2000**, *50*, 1308–1320. [\[CrossRef\]](#) [\[PubMed\]](#)
13. Han, J.S.; Moon, K.J.; Lee, S.J.; Kim, Y.J.; Ryu, S.Y.; Cliff, S.S.; Yi, S.M. Size-Resolved Source Apportionment of Ambient Particles by Positive Matrix Factorization at Gosan Background Site in East Asia. *Atmos. Chem. Phys.* **2006**, *6*, 211–223. [\[CrossRef\]](#)
14. Han, S.; Joo, H.-S.; Song, H.-J.; Lee, S.-B.; Han, J.-S. Source Apportionment of PM_{2.5} in Daejeon Metropolitan Region during January and May to June 2021 in Korea Using a Hybrid Receptor Model. *Atmosphere* **2022**, *13*, 1902. [\[CrossRef\]](#)
15. Han, S.; Joo, H.; Kim, K.; Cho, J.; Moon, K.; Han, J. Modification of Hybrid Receptor Model for Atmospheric Fine Particles (PM_{2.5}) in 2020 Daejeon, Korea, Using an ACERWT Model. *Atmosphere* **2024**, *15*, 477. [\[CrossRef\]](#)
16. Kang, S.; Choi, S.; Ban, J.; Kim, K.; Singh, R.; Park, G.; Kim, M.-B.; Yu, D.-G.; Kim, J.-A.; Kim, S.-W.; et al. Chemical Characteristics and Sources of PM_{2.5} in the Urban Environment of Seoul, Korea. *Atmos. Pollut. Res.* **2022**, *13*, 101568. [\[CrossRef\]](#)
17. Yi, S.-M.; Hwang, I. Source Identification and Estimation of Source Apportionment for Ambient PM₁₀ in Seoul, Korea. *Asian J. Atmos. Environ.* **2014**, *8*, 115–125. [\[CrossRef\]](#)
18. Jo, H.-Y.; Kim, C.-H. Identification of Long-Range Transported Haze Phenomena and Their Meteorological Features over Northeast Asia. *J. Appl. Meteorol. Climatol.* **2013**, *52*, 1318–1328. [\[CrossRef\]](#)
19. Park, H.-Y.; Ahn, J.-Y.; Hong, S.-C.; Lee, J.-B.; Cho, S.-Y. The Formation and Transport of HNO₃ over the Yellow Sea and Its Impact on the January 2018 PM_{2.5} Episode in Seoul. *Environ. Sci. Atmos.* **2024**, *4*, 670–684. [\[CrossRef\]](#)
20. Ju, S.; Yu, G.H.; Park, S.; Lee, J.Y.; Lee, S.; Jee, J.; Lee, K.; Lee, M. Pollution Characteristics of PM_{2.5} Measured during Fall at a Seosan Site in Chungcheong Province. *J. Korean Soc. Atmos. Environ.* **2020**, *36*, 329–345. [\[CrossRef\]](#)
21. Park, T.; Ban, J.; Kang, S.; Ghim, Y.S.; Shin, H.-J.; Park, J.S.; Park, S.M.; Moon, K.J.; Lim, Y.-J.; Lee, M.-D.; et al. Chemical Characteristics of PM₁ using Aerosol Mass Spectrometer at Baengnyeong Island and Seoul Metropolitan Area. *KOSAE* **2018**, *34*, 430–446. [\[CrossRef\]](#)
22. Ju, H.; Kim, H.C.; Kim, B.-U.; Ghim, Y.S.; Shin, H.J.; Kim, S. Long-term Trend Analysis of Key Criteria Air Pollutants over Air Quality Control Regions in South Korea using Observation Data and Air Quality Simulation. *KOSAE* **2018**, *34*, 101–119. [\[CrossRef\]](#)
23. Park, S.-Y.; Kim, C.-H. Identification of Long-Range Transported Air Pollution Indicators over Northeast Asia. *J. Korean Soc. Atmos. Environ.* **2013**, *29*, 38–55. [\[CrossRef\]](#)
24. NIER Air Pollution Monitoring Network Installation and Operation Guidelines 2022. Available online: https://www.airkorea.or.kr/web/board/3/769/?pMENU_NO=145&page=+1 (accessed on 30 August 2024).
25. NIER Establishment of Guidelines for the PMF Modeling and Applications 2021. Available online: https://books.google.co.kr/books/about/%EC%88%98%EC%9A%A9%EB%AA%A8%EB%8D%B8_%EC%9A%B4%EC%98%81%EB%B0%A9%EB%B2%95%EC%9D%98_%ED%91%9C%EC%A4%80%ED%99%94.html?id=PYenzwEACAAJ&redir_esc=y (accessed on 30 August 2024).
26. Lee, H.; Kim, N.; Jo, M.; Lee, S.; Choi, J.; Kang, K.; Choi, S. Characteristics of PM_{2.5} Pollution and Long-range Atmospheric Transport in Background Areas (Baengnyeong and Jeju Islands). *KOSAE* **2022**, *38*, 524–541. [\[CrossRef\]](#)
27. Lee, H. Jo Isotopic Characteristics of Nitrate Aerosols for Tracing PM_{2.5} Sources in South Korea. Ph.D. Thesis, Seoul National University, Seoul, Republic of Korea, 2019.
28. Oh, H.-R.; Ho, C.-H.; Kim, J.; Chen, D.; Lee, S.; Choi, Y.-S.; Chang, L.-S.; Song, C.-K. Long-Range Transport of Air Pollutants Originating in China: A Possible Major Cause of Multi-Day High-PM₁₀ Episodes during Cold Season in Seoul, Korea. *Atmos. Environ.* **2015**, *109*, 23–30. [\[CrossRef\]](#)
29. Draxler, R.R.; Rolph, G.D. HYSPLIT (HYbrid Single-ParticleLagrangian Integrated Trajectory) Model Access via NOAA ARL READY Website. Available online: <https://www.arl.noaa.gov/hysplit/> (accessed on 27 July 2024).
30. Huang, X.; Liu, Z.; Zhang, J.; Wen, T.; Ji, D.; Wang, Y. Seasonal Variation and Secondary Formation of Size-Segregated Aerosol Water-Soluble Inorganic Ions during Pollution Episodes in Beijing. *Atmos. Res.* **2016**, *168*, 70–79. [\[CrossRef\]](#)
31. Thorpe, A.; Harrison, R.M. Sources and Properties of Non-Exhaust Particulate Matter from Road Traffic: A Review. *Sci. Total Environ.* **2008**, *400*, 270–282. [\[CrossRef\]](#)
32. Park, J.; Kim, H.; Kim, Y.; Heo, J.; Kim, S.-W.; Jeon, K.; Yi, S.-M.; Hopke, P.K. Source Apportionment of PM_{2.5} in Seoul, South Korea and Beijing, China Using Dispersion Normalized PMF. *Sci. Total Environ.* **2022**, *833*, 155056. [\[CrossRef\]](#)
33. Viana, M.; Pandolfi, M.; Minguillón, M.C.; Querol, X.; Alastuey, A.; Monfort, E.; Celades, I. Inter-Comparison of Receptor Models for PM Source Apportionment: Case Study in an Industrial Area. *Atmos. Environ.* **2008**, *42*, 3820–3832. [\[CrossRef\]](#)
34. Liu, T.; Hu, B.; Yang, Y.; Li, M.; Hong, Y.; Xu, X.; Xu, L.; Chen, N.; Chen, Y.; Xiao, H.; et al. Characteristics and Source Apportionment of PM_{2.5} on an Island in Southeast China: Impact of Sea-Salt and Monsoon. *Atmos. Res.* **2020**, *235*, 104786. [\[CrossRef\]](#)
35. Helble, J.J. A Model for the Air Emissions of Trace Metallic Elements from Coal Combustors Equipped with Electrostatic Precipitators. *Fuel Process. Technol.* **2000**, *63*, 125–147. [\[CrossRef\]](#)
36. Lee, J.H.; Yoshida, Y.; Turpin, B.J.; Hopke, P.K.; Poirrot, R.L.; Liroy, P.J.; Oxley, J.C. Identification of Sources Contributing to Mid-Atlantic Regional Aerosol. *J. Air Waste Manag. Assoc.* **2002**, *52*, 1186–1205. [\[CrossRef\]](#) [\[PubMed\]](#)

37. Hwang, K.-W.; Kim, D.-Y.; Jin, S.-J.; Kim, I.-H. A Study on the Factors Influencing Air Pollutions in the Islands of Korean Peninsula: Focusing on the Case of Ulleung, Jeju, and Baengnyong Island. *J. Korea Acad. Ind. Coop. Soc.* **2020**, *21*, 814–824. [[CrossRef](#)]
38. Kang, E.; Lee, M.; Brune, W.H.; Lee, T.; Park, T.; Ahn, J.; Shang, X. Photochemical Aging of Aerosol Particles in Different Air Masses Arriving at Baengnyeong Island, Korea. *Atmos. Chem. Phys.* **2018**, *18*, 6661–6677. [[CrossRef](#)]
39. Nojiri, R.; Osada, K.; Kurosaki, Y.; Matsuoka, M.; Sadanaga, Y. Variations in Gaseous Nitric Acid Concentrations at Tottori, Japan: Long-Range Transport from the Asian Continent and Local Production. *Atmos. Environ.* **2022**, *274*, 118988. [[CrossRef](#)]
40. Zhang, Z.; Lu, B.; Liu, C.; Meng, X.; Jiang, J.; Herrmann, H.; Chen, J.; Li, X. Nitrate Pollution Deterioration in Winter Driven by Surface Ozone Increase. *NPJ Clim. Atmos. Sci.* **2024**, *7*, 160. [[CrossRef](#)]
41. Kim, K.; Lee, C.; Choi, D.; Han, S.; Eom, J.; Han, J. A Study on the Formation Reactions and Conversion Mechanisms of HONO and HNO₃ in the Atmosphere of Daejeon, Korea. *Atmosphere* **2024**, *15*, 267. [[CrossRef](#)]
42. Lurmann, F.W.; Brown, S.G.; McCarthy, M.C.; Roberts, P.T. Processes Influencing Secondary Aerosol Formation in the San Joaquin Valley during Winter. *J. Air Waste Manag. Assoc.* **2006**, *56*, 1679–1693. [[CrossRef](#)]

Disclaimer/Publisher’s Note: The statements, opinions and data contained in all publications are solely those of the individual author(s) and contributor(s) and not of MDPI and/or the editor(s). MDPI and/or the editor(s) disclaim responsibility for any injury to people or property resulting from any ideas, methods, instructions or products referred to in the content.